



Mechanism of selective alcohol oxidation to aldehydes on gold catalysts: Influence of surface roughness on reactivity

Mercedes Boronat^a, Avelino Corma^{a,*}, Francesc Illas^b, Juan Radilla^{b,c}, Tania Ródenas^a, María J. Sabater^a

^a Instituto de Tecnología Química, Universidad Politécnica de Valencia – Consejo Superior de Investigaciones Científicas, Av. los Naranjos, s/n, 46022 Valencia, Spain

^b Departament de Química Física & Institut de Química Teòrica i Computacional (IQTCUB), Universitat de Barcelona, C/Martí i Franquès 1, 08028 Barcelona, Spain

^c Departamento de Ciencias Básicas, Área de Química, Universidad Autónoma Metropolitana-Azcapotzalco, Av. San Pablo 180, CP. 02200 México, D.F., Mexico

ARTICLE INFO

Article history:

Received 6 October 2010

Revised 18 November 2010

Accepted 19 November 2010

Available online 6 January 2011

Keywords:

Catalysis

Au

DFT

Alcohol oxidation

Selectivity

ABSTRACT

The complete reaction pathway for the selective alcohol oxidation to aldehyde has been obtained from periodic density functional theory (DFT) calculations on a series of catalyst models having Au atoms with different coordination number. A clear trend exists in the reactivity of the surfaces: it increases with decreasing the Au coordination number, suggesting that a distribution of Au sites with different activity might exist on the surface of real catalysts. This hypothesis emerging from the theoretical study has been experimentally confirmed by measuring the kinetics of benzyl alcohol oxidation on a series of Au/MgO catalysts having different particle diameter and therefore different concentration and distribution of low coordinated Au sites.

© 2010 Elsevier Inc. All rights reserved.

1. Introduction

The selective oxidation of alcohols to carbonylic compounds over heterogeneous recyclable catalysts is an important process in green organic chemistry [1–3]. Most efforts in recent years have focused on the aerobic oxidation that uses molecular oxygen as oxidant generating water as the only byproduct, and good results have been obtained with metal-based catalysts containing Ru [4,5], Ag [6,7], Cu [8,9], Au [10–14] or Pd [15–17]. Different studies [1–6,11,14] agree that the mechanism for aerobic alcohol oxidation starts with the formation of a metal-alkoxy species that, in a second step, suffers a β -hydride elimination giving rise to the carbonylic product and a metal-hydride intermediate. Although it has been shown that in some cases the alkoxy intermediate is not formed on the metal particle but on the oxide support [6,10,14], there are many other examples demonstrating that naked metal particles in colloidal solutions [18] or supported on carbon [7,19,20], silica [12,14,16,17] or metal organic frameworks (MOF) [21,22] are highly active for alcohol oxidation, even in the absence of a base [21]. Moreover, instead of using molecular oxygen to finally obtain nontoxic but valueless H₂O as a byproduct, it would be more interesting to use the carbonyl compound and metal-hydride species obtained from oxidative alcohol dehydrogenation in consecutive reactions yielding products of high added value. In this sense, it

has been recently reported that a bifunctional Pd/MgO catalyst performs the one-pot selective N-monoalkylation of amines with alcohols. This occurs through a series of consecutive steps in a cascade mode involving alcohol dehydrogenation, condensation of the carbonyl compound with the amine yielding an imine, and hydro-generation of the imine with the hydrogen atoms from the metal hydride obtained in the first step [23]. Thus, it is of interest to understand the mechanism of the metal-catalyzed dehydrogenation of alcohols in the absence of O₂ or of a base.

In the case of gold-catalyzed alcohol oxidation, it has been found that catalytic activity and selectivity depend on metal particle size, and that the best performance is exhibited by the smaller particles [14,22,24]. This observation could be explained by taking into account that, as the particle size decreases, the number of low coordinated atoms that are considered to be the active sites in many gold-catalyzed reactions increases. To confirm this hypothesis, we have attacked the problem from two different and complementary perspectives. On one hand, the complete mechanism of ethanol oxidation to ethanal has been theoretically investigated by means of periodic density functional theory (DFT) based calculations on a series of catalyst models having Au atoms with different coordination number. On the other hand, different gold catalysts with particle size between 2 and 10 nm have been synthesized, and the kinetics of benzyl alcohol dehydrogenation have been measured. By combining the theoretical and experimental results, it is shown that the presence of low coordinated Au atoms enhances alcohol adsorption on the catalyst and decreases the

* Corresponding author. Fax: +34 96 387 79 444.

E-mail address: acorma@itq.upv.es (A. Corma).

activation barrier for dehydrogenation, thus explaining the influence of particle size on the oxidation activity of gold catalysts.

2. Experimental section

2.1. Catalyst preparation

Au–MgO catalysts were prepared by impregnation of 1 g of a MgO sample with a surface area of 670 m²/g from Nanoscale Materials with 10 ml of HAuCl₄·3H₂O solutions containing different amounts of gold (0.4%, 0.8%, 1.5%, 3.0%, 5.0%, and 10% weight) under stirring for 2 h. The solvent was evaporated at reduced pressure, and the solid was dried at 333 K during 6 h. Finally, the sample was calcined at 573 K under air flow for 3 h and then under N₂ flow for 3 h.

2.2. Kinetic experiments

The kinetic experiments were carried out by working at different initial concentrations of benzyl alcohol (0.4, 0.8, 1.0, 1.2, and 1.6 mmol/ml) and with a catalyst concentration corresponding in all cases to 0.0075 mmol of Au. The reactants and the catalyst were introduced into an autoclave containing 20 μL n-dodecane and 1 ml trifluorotoluene. Once closed, the reactor was purged with N₂ and the reaction mixture was heated to the desired temperature (413, 423, 453, 463, 473, and 483 K) and stirred at 500 r.p.m. during the whole experiment. The reaction was monitored by GC.

2.3. Model catalysts and computational details

Perfect and stepped single crystal Au surfaces as well as an isolated Au nanoparticle were represented by the usual periodic slab model approach, using super cells large enough to avoid interaction either between the periodically repeated gold surfaces (or particles) or between the periodically repeated adsorbates. The extended surfaces were modeled by (2 × 2) super cell slabs containing a material thickness of ~8 Å and a vacuum region of ~12 Å, as shown in Fig. 1. The slab model for the Au(1 1 1) surface contains 16 atoms arranged in four layers. The stepped Au(5 1 1) surface has (1 0 0) terraces and (1 1 1) steps, and the unit cell contains 44 atoms distributed in eleven metallic layers. Another stepped surface hereafter termed *Au-rod* and containing 36 atoms in the unit cell was built from the 4 × 2 unit cell of the (1 0 0) slab as described in previous work [25]. The *Au-rod* model has two types of (1 0 0) terraces (upper and lower) separated by a monoatomic step with (1 1 1) orientation, and it has been included in

the study because its behavior in relation to ethoxy adsorption is not completely equivalent to that of the Au(5 1 1) surface. Finally, an Au₃₈ nanoparticle having a typical cuboctahedral shape and ~1 nm diameter was placed in a 20 × 20 × 20 Å cubic box, large enough to allow a separation larger than 10 Å between periodically repeated particles. In the geometry optimization of the extended surfaces the uppermost layers were fully relaxed, while the atomic positions of the two innermost layers were kept fixed as in the bulk to provide an adequate environment to the surface atoms. In the case of the Au₃₈ nanoparticle, the positions of all atoms were always fully relaxed.

Ethanol adsorption on the different Au models described above was considered and the complete reaction pathway for its oxidation to acetaldehyde was obtained. This includes geometry optimization of the adsorbed ethanol reactant, the ethoxy reaction intermediate plus a hydrogen atom, the adsorbed acetaldehyde final reaction product plus two adsorbed hydrogen atoms, and the transition states connecting all these minima. In all calculations, the atomic positions of C, O, and H atoms, as well as those of the Au atoms in the uppermost layers of the surfaces as described earlier and all Au atoms in the nanoparticle were fully relaxed.

Total energies were obtained from periodic density functional calculations using the Perdew–Wang (PW91) implementation of the Generalized Gradient Approach (GGA) for the exchange–correlation potential [26–28]. The valence electron density was expanded in a plane wave basis set with a kinetic energy cutoff of 415 eV. The effect of the core electrons in the valence density was taken into account by means of the Projected Augmented Wave (PAW) formalism [29] as implemented by Kresse and Joubert [30] in the VASP code [31,32]. Integration in the reciprocal space was carried out using a 5 × 5 × 1 mesh of special Monkhorst–Pack *k*-points [33] for the gold surfaces, while calculations with the gold nanoparticle were carried out at the Γ *k*-point of the Brillouin zone. The atomic positions were optimized by means of a conjugate-gradient algorithm until atomic forces were smaller than 0.01 eV/Å. Transition states were located using the DIMER algorithm [34,35] and stationary points thus found were characterized by pertinent frequency analysis calculations. Vibrational frequencies were calculated by diagonalizing the block Hessian matrix corresponding to displacements of the C, O, and H atoms of the organic fragment, and the zero point vibrational correction was added to the calculated energies. Charge distributions were estimated using the quantum theory of atoms in molecules (AIM) of Bader using the algorithm developed by Henkelman et al. [36,37]. Calculations have been carried out without taking spin polarization into account except when needed, such as in the case of the isolated O₂ molecule.

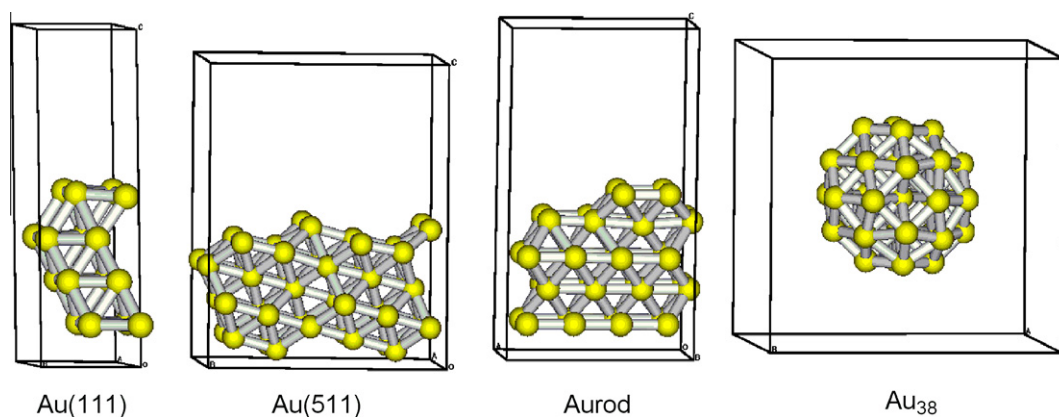


Fig. 1. Side view of the unit cell of the different gold surfaces and Au₃₈ nanoparticle employed in this work.

3. Results and discussion

3.1. Theoretical study of the reaction mechanism

The mechanism of selective oxidation of ethanol to ethanal consists of two elementary steps: (1) dehydrogenation of the hydroxyl group of adsorbed ethanol to give an ethoxy species and a hydrogen atom adsorbed on the metal surface and (2) transfer of a second hydrogen atom from the C atom bonded to O (H_β) in the ethoxy intermediate to the Au surface, yielding ethanal and a second hydrogen atom adsorbed on the catalyst surface. The structures involved in the reaction mechanism on Au(5 1 1) surface, together with a definition of the most relevant geometric parameters to be analyzed, are depicted in Fig. 2. Table 1 summarizes the optimized values of these parameters on all catalyst models considered. The calculated adsorption, reaction and activation energies are given in Table 2, and the energy profiles obtained on the different catalyst models are schematized in Fig. 3.

Ethanol adsorbs on all surfaces and on the Au_{38} particle with the O on top of an Au atom, although adsorption on highly coordinated Au atoms present at regular surfaces is fairly weak. Therefore, only sites located at the step edges and having coordination number 7 were considered for ethanol adsorption on the Au(5 1 1) surface and on the *Au-rod* model. On the Au_{38} nanoparticle, ethanol adsorption was found to occur at corner sites having coordination number 6. The bond lengths and angles in ethanol are practically unmodified upon adsorption, but the Au–O distance becomes shorter as the coordination number of the Au atom with which ethanol is interacting decreases. The calculated adsorption energies (E_{ads} in Table 2 and Fig. 3) follow the opposite trend and increase in a continuous way from Au(1 1 1) to Au_{38} . However, the E_{ads} value obtained on the *Au-rod* model is considerably larger than on the stepped Au(5 1 1) surface, indicating that coordination number is not the only factor determining energies. When comparing the step sites in the Au(5 1 1) and *Au-rod* models, one can see that the coordination and local environment around the adsorption site is similar along the step, but quite different across the step,

Table 1

Optimized values (in Å) of the most relevant distances of the structures involved in the mechanism of ethanol oxidation on gold. The atom labeling is given in Fig. 2.

	Au(1 1 1)	Au(5 1 1)	<i>Au-rod</i>	Au_{38}
<i>Ethanol</i>				
rAu–O	3.231	2.696	2.690	2.468
rOH	0.978	0.978	0.980	0.979
rAu–H	2.820	2.819	2.835	3.054
rCO	1.439	1.449	1.449	1.455
<i>TS1</i>				
rAu–O	2.167	2.275, 2.323	2.335	2.087, 3.348
rOH	1.927	1.703	1.587	2.045
rAu–H	1.823	1.671	1.908	1.619
rCO	1.418	1.441	1.440	1.425
<i>Ethoxy + H</i>				
rAu–O	2.277, 2.361	2.201, 2.194	2.199	2.198, 2.202
rAu–H	1.875, 1.944	1.780	1.777	1.816
rAu– H_β	2.943	3.312	3.220	3.365
rCO	1.425	1.437	1.441	1.434
<i>TS2</i>				
rAu–O	2.411	2.271	2.273	2.202
rC– H_β	1.614	1.616	1.618	1.698
rAu– H_β	1.712	1.689	1.692	1.685
rCO	1.274	1.279	1.280	1.279
<i>Aldehyde + 2H</i>				
rAu–O	4.735	2.757	3.010	2.375
rCO	1.223	1.224	1.224	1.235

Table 2

Calculated adsorption, activation and reaction energies (in kcal mol⁻¹) involved in the reaction mechanism schematized in Fig. 3. The negative values indicate that the process is exothermic.

	Au(1 1 1)	Au(5 1 1)	<i>Au-rod</i>	Au_{38}
E_{ads}	-2.9	-4.9	-9.6	-12.1
E_{act1}	32.7	27.9	24.1	19.2
$\Delta E1$	27.2	14.0	11.4	2.1
E_{act2}	5.2	10.2	13.7	9.7
$\Delta E2$	-16.0	-1.4	-1.3	1.7

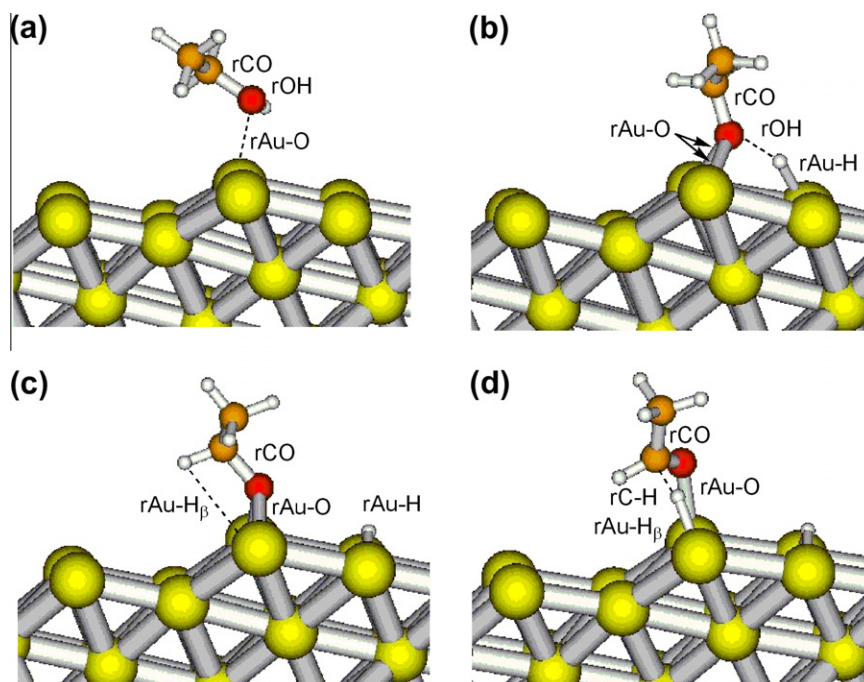


Fig. 2. Structures involved in the reaction mechanism on Au(5 1 1): (a) adsorbed ethanol, (b) transition state for the first (TS1) dehydrogenation, (c) co-adsorbed ethoxy and H and (d) transition state for the second (TS2) dehydrogenation.

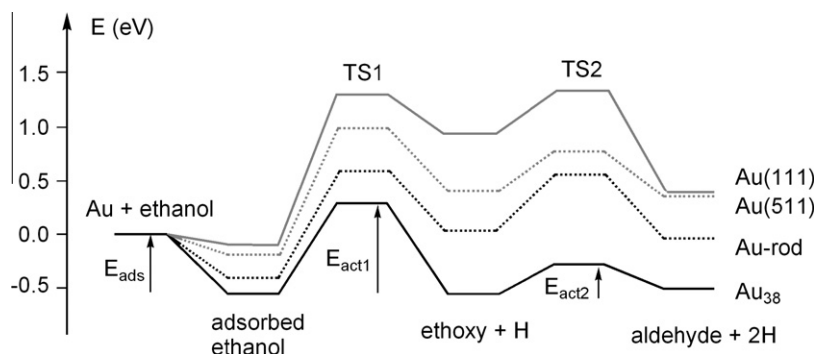


Fig. 3. Calculated energy profile for the dehydrogenation of ethanol on different gold catalyst models.

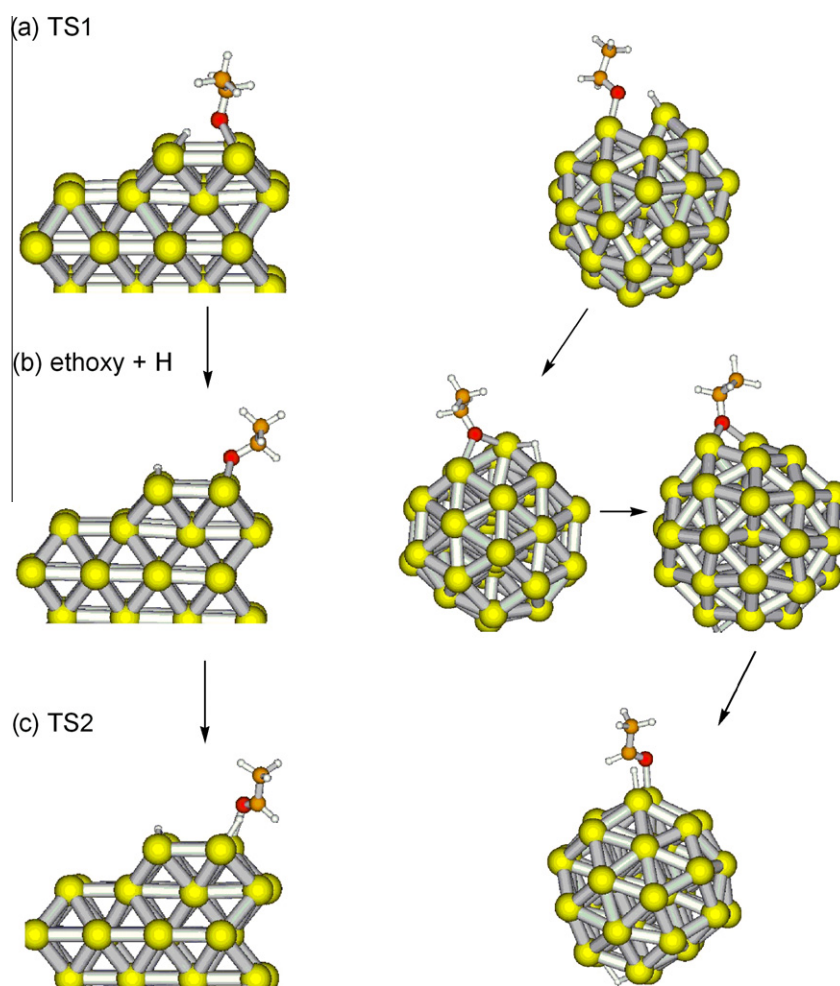


Fig. 4. Structures involved in the reaction mechanism on the *Au-rod* model (left) and the Au_{38} nanoparticle (right): (a) transition state for the first dehydrogenation TS1, (b) co-adsorbed ethoxy and H and (c) transition state for the second dehydrogenation TS2.

because the (1 0 0) terraces in the $Au(5\ 1\ 1)$ surface are larger than in the *Au-rod* model. The coordination of the Au atoms next to those in the step in the $Au(5\ 1\ 1)$ surface is 8, while in the *Au-rod* model, the Au atoms next to those in the step where ethanol is adsorbed belong to another step and are therefore coordinated to 7 Au atoms. As a result, the *Au-rod* model is more flexible than the $Au(5\ 1\ 1)$ surface and allows a better relaxation upon molecular adsorption, which is reflected in larger adsorption energies and lower activation barriers (see Table 2).

In the transition state for the first elementary step of the ethanol oxidation mechanism, TS1, the OH bond is broken and the hydrogen atom of the hydroxyl group and the resulting ethoxy fragment bind to different sites on the Au surfaces and nanoparticles. The optimized OH (1.5–2.0 Å) and Au–H (1.6–1.9 Å) bond lengths summarized in Table 2 reflect the hydrogen transfer process. Moreover, the Au–O distances become shorter, while the CO bond remains almost unaltered. After dissociation of the OH group, the ethoxy fragment adsorbs with the C–O bond almost

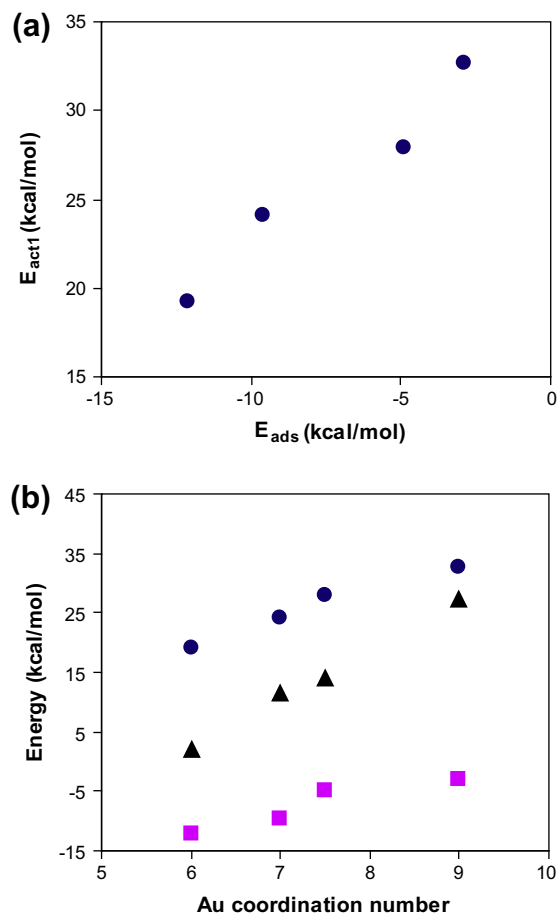


Fig. 5. Plots of: (a) activation energy of the rate-determining step versus energy of adsorption energy of ethanol on the different gold catalyst models and (b) adsorption (squares), activation (circles) and reaction (triangles) energies versus Au coordination number.

perpendicular to the surface and the oxygen atom on a 3-fold hollow position on Au(1 1 1) surface, and with the oxygen atom interacting with two atoms of the step edge in a bridge configuration on the Au(5 1 1), *Au-rod* and Au₃₈ models (see Figs. 2 and 4). In all cases, the calculated Au–O distances are ~ 2.2 Å.

The calculated activation energies reported in Table 2 clearly show that this dehydrogenation is the rate-determining step of the reaction. E_{act1} values decrease from 32.7 kcal mol⁻¹ for the perfect Au(1 1 1) surface to 19.2 kcal mol⁻¹ on the Au₃₈ nanoparticle and are not equivalent in the stepped Au(5 1 1) and *Au-rod* surfaces. A similar but still more pronounced trend is found for the reaction energies $\Delta E1$, which reflect the higher stabilization of the ethoxy + H intermediate as the coordination of Au atoms on the active site decrease. As depicted in Fig. 2, after dissociation of

the OH bond on the Au(5 1 1) surface, the H atom occupies a bridge position between two Au atoms of the Au(1 0 0) terrace having coordination number 8. However, the same process on the *Au-rod* model leaves the H atom adsorbed on the step edge, in a more stable situation. The dissociation of the OH group of ethanol on the Au₃₈ nanoparticle, depicted in Fig. 4, deserves a more detailed description. Despite all our efforts to find a transition state TS1 equivalent to those obtained on Au(5 1 1) and *Au-rod* models, in which OH dissociation occurs through the square formed by the Au atoms of the Au(1 0 0) terrace, the breaking of the hydroxyl group on Au₃₈ nanoparticle occurs at the edge of the Au(1 0 0) upper facet of the particle, and only involves in a direct way two Au atoms. Thus, the OH distance in TS1 on Au₃₈ is the longest, the H atom is on top of one Au atom in a corner position, and the ethoxy fragment is on top of a second corner Au atom. The distance between these two Au atoms, which were initially bonded with a Au–Au bond length of 2.824 Å, increases to 3.828 Å in the transition state and reaches a value of 3.479 Å in the ethoxy + H intermediate. This large geometrical distortion of the particle is energetically compensated by the interactions with the organic fragments, leading to the lowest activation and reaction energies in the series of model catalysts studied. This is an important point since it shows that the fluxional structure of the Au nanoparticle is also a key factor in reducing the activation energy toward O–H dissociation. It is also important to remark that, after dissociation of the hydroxyl group, the H atom occupies a bridge position between two Au atoms beside adsorbed ethoxy, but can easily move to the particle surface or to other more stable bridge positions farther away from ethoxy. The energy difference between the least and the most stable structures obtained for ethoxy + H intermediate, depicted in Fig. 4, is ~ 3 kcal mol⁻¹, and the data given in Table 1 correspond to the most stable system, which has also been considered as starting point for the second deprotonation step.

The optimized structure of TS2 is almost similar on all surfaces and particles considered. The ethoxy fragment is displaced from its bridge position and moves closer to one of the Au atoms to which it was bonded, leaving the other Au atom free to interact with the H_β that is being abstracted. The hydrogen atom being transferred to the Au surface is halfway between the C and the Au atoms, with optimized C–H_β and Au–H_β distances between 1.6 and 1.7 Å. At the same time, the CO bond length shortens to ~ 1.28 Å, indicating that it is being converted into a carbonyl group. Finally, ethanal is formed and desorbs, leaving two hydrogen atoms occupying 3-fold hollow positions on Au(1 1 1) surface and bridge positions on the stepped surfaces and the nanoparticle. The activation barriers involved in the abstraction of the H_β are smaller than those corresponding to the dehydrogenation of the hydroxyl group, and do not seem to follow any clear trend with the coordination of the Au atoms or surface roughness.

In order to rationalize the results obtained, we have searched for relationships between adsorption, reaction and activation energies for the rate-determining step and the coordination of the Au atoms involved in the process. As discussed earlier, Au atoms in

Table 3
Characterization data (gold loading in% weight and measured by ICP-OES analysis, particle diameter in nm and area in (m²/g) and calculated turnover frequencies (TOF in h⁻¹) for the different catalysts considered in this work together with calculated adsorption enthalpies of benzyl alcohol (ΔH) and activation energies (E_{act}) for benzyl alcohol oxidation.

Au (%)	Au (ICP-OES)	Diameter (nm)	Area (m ² /g)	TOF (h ⁻¹) ^a	ΔH (kcal mol ⁻¹)	E_{act} (kcal mol ⁻¹)
0.4	0.3784	1.9	212.2	113	7.3 ± 1.3	7.9 ± 1.3
0.8	0.8216	3.3	175.9	324	6.5 ± 0.9	8.6 ± 1.1
1.5	1.4371	4.1	53.3	74	5.2 ± 0.3	9.6 ± 0.6
3.0	2.9360	5.9	52.6	31	4.7 ± 0.6	9.8 ± 0.8
5.0	5.1321	8.1	38.6	30	4.3 ± 0.5	10.0 ± 1.0
10.0	10.1885	9.7	37.9	26	3.8 ± 0.3	10.4 ± 0.6

^a Calculated at $T = 453$ K and [alcohol] = 1 mmol/L.

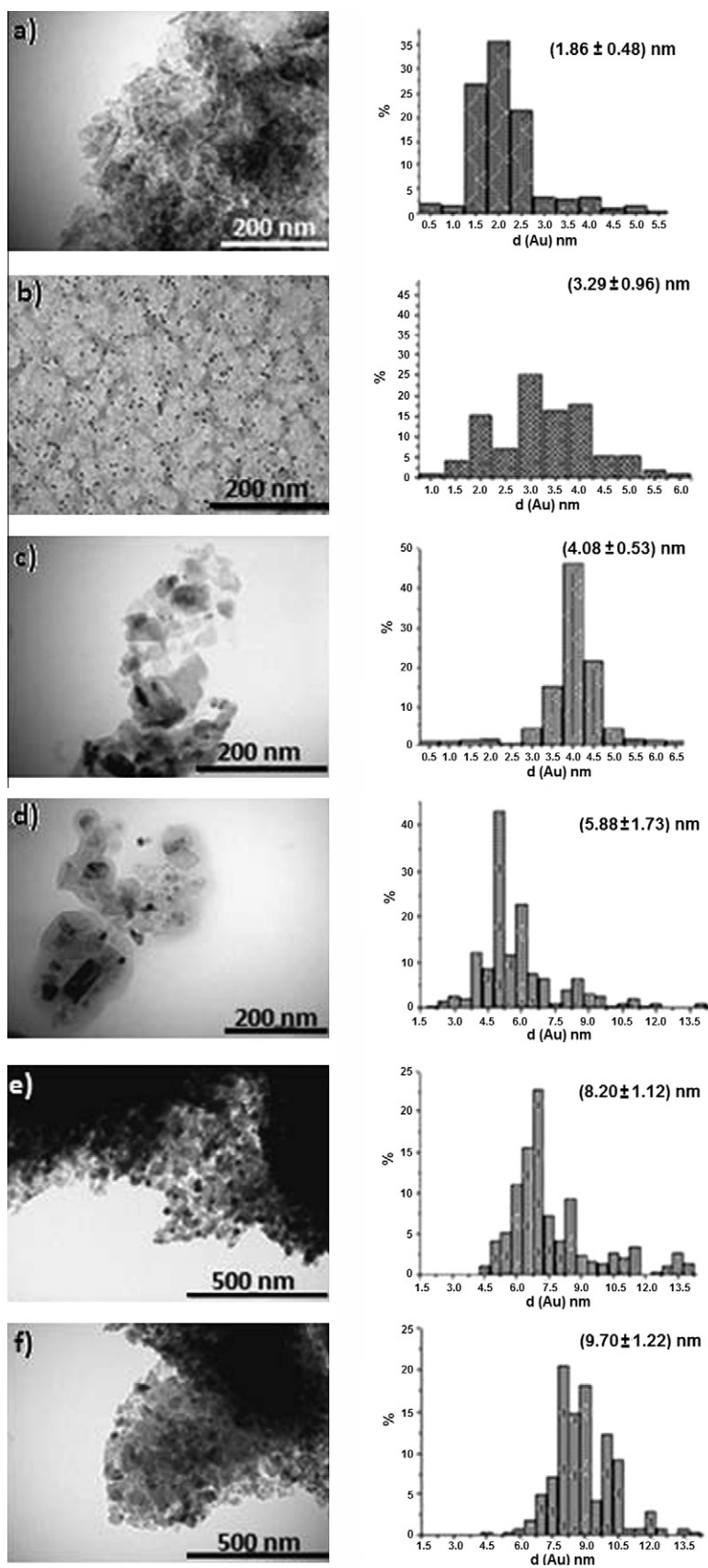


Fig. 6. TEM micrographs and particle size distribution of Au/MgO catalysts with different gold loading: (a) 0.4%wt, (b) 0.8%wt, (c) 1.5%wt, (d) 3.0%wt, (e) 5.0%wt and (f) 10.0%wt.

the step edge of the Au(5 1 1) and Au-rod models have coordination number 7, but Au atoms next to those in the step and also directly participating in the mechanism have coordination number 8 on Au(5 1 1), and therefore an average coordination number of 7.5 has been applied to Au(5 1 1) surface. The relevant relationships thus found are depicted in Fig. 5. On one hand, we observe that ethanol adsorption energies and activation barriers are linearly correlated, evidencing that a Brønsted–Evans–Polanyi (BEP) relationship [38,39] holds for this elementary step (Fig. 5a). Therefore, the term reactivity can be in this case associated either to a stronger interaction with adsorbates or to a lower activation barrier involved in the reaction. On the other hand, and as deduced from the discussion above, there is a clear trend in the reactivity of the model surfaces; it increases with decreasing the Au coordination number (Fig. 5b). This means that not all active sites are equivalent and that real gold catalysts might have heterogeneous surfaces with Au atoms in different coordination state showing different reactivity towards alcohol dehydrogenation. In order to confirm this hypothesis, a series of Au catalysts with different particle diameter were prepared and characterized, and their catalytic activity for the oxidation of benzyl alcohol to benzaldehyde was measured. These experiments will be described in detail in the forthcoming section.

3.2. Kinetic study of the reaction mechanism

The kinetics of the dehydrogenation of benzyl alcohol to benzaldehyde on a series of Au/MgO catalysts containing different gold loading and particle size were studied using the initial reaction rate method. The characterization data summarized in Table 3 and the TEM images shown in Fig. 6 indicate that the amount of gold in the catalyst determines the particle size, so that the higher the gold loading the larger the metal particles are.

The kinetic rate equation was deduced by considering that benzyl alcohol adsorbs on the gold nanoparticles with a equilibrium constant K_{ads} defined as:

$$K_{\text{ads}} = \frac{[\text{alcohol}]_{\text{ads}}}{[\text{alcohol}][\text{cat}]} \quad (1)$$

and that the mechanism for adsorbed alcohol dehydrogenation involves two consecutive steps according to:



where k_1 is the kinetic constant corresponding to the first dehydrogenation of the alcohol to give an alkoxy intermediate and a hydrogen atom adsorbed on the Au surface and k_2 is the kinetic constant corresponding to the second dehydrogenation step yielding the aldehyde and a new hydrogen atom adsorbed on the gold surface. However, in practice, these two steps cannot be measured independently and a global kinetic constant k_c was employed in the kinetic rate equation:

$$r_0 = \frac{K_{\text{ads}}k_c[\text{cat}][\text{alcohol}]_0}{1 + K_{\text{ads}}[\text{alcohol}]_0} \quad (4)$$

which after linearization is converted into:

$$\frac{1}{r_0} = \frac{1}{K_{\text{ads}}k_c[\text{cat}][\text{alcohol}]_0} + \frac{1}{k_c[\text{cat}]} \quad (5)$$

Thus, by plotting the inverse of the initial reaction rate versus the inverse of the initial concentration of benzyl alcohol, a straight line should be obtained, and from the slope and intercept at the origin of the fitted equation, the values of k_c and K_{ads} can be deduced. The fit of the experimental data to Eq. (5) for the different catalysts considered in this work at different temperatures is good, as depicted in Fig. S1. The calculated kinetic and adsorption constants are summarized in Table S1 in the Supporting information.

Activation energies E_{act} were calculated from the measured rate constants at different temperatures according to the Arrhenius equation:

$$k_c = Ae^{-E_{\text{act}}/RT} \quad (6)$$

$$\ln(k_c) = \ln(A) - \frac{E_{\text{act}}}{R} \left(\frac{1}{T}\right) \quad (7)$$

where A is the pre-exponential factor, R is the molar gas constant and T is the reaction temperature. Adsorption enthalpies ΔH of benzyl alcohol on the different catalysts were calculated using the van't Hoff equation:

$$\ln(K_{\text{ads}}) = -\frac{\Delta H}{R} \left(\frac{1}{T}\right) + \frac{\Delta S}{R} \quad (8)$$

where R is the molar gas constant, T is the reaction temperature, and ΔS is the entropy change of the reaction. Fig. 7 shows the variation of the kinetic k_c and adsorption K_{ads} constants with temperature. The fitting of the experimental data to Eqs. (7) and (8) is good in all cases, and the calculated activation energies and adsorption enthalpies are summarized in Table 3. Activation energies linearly increase with increasing particle size, while benzyl alcohol adsorp-

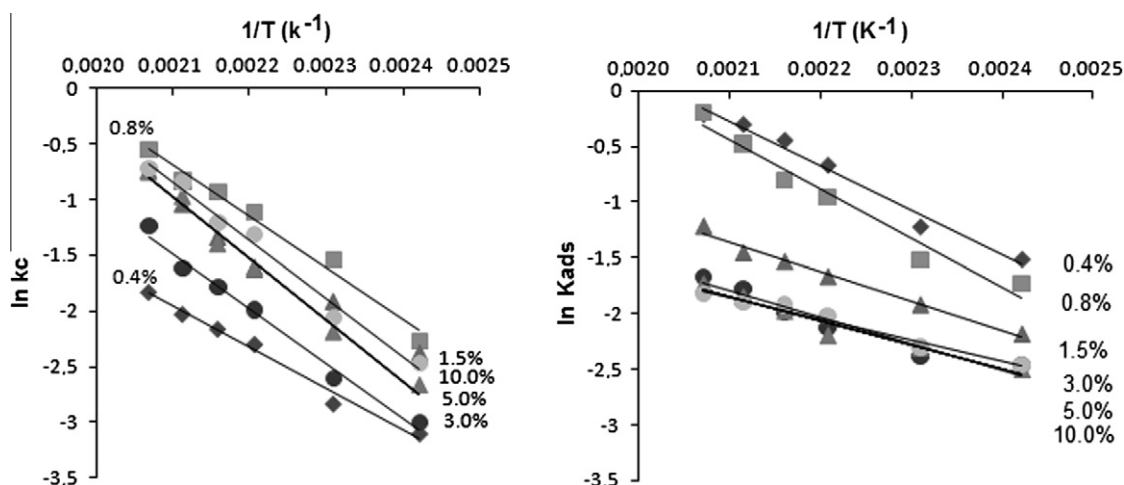


Fig. 7. Variation of the kinetic constants k_c and adsorption constants K_{ads} for benzyl alcohol oxidation with temperature on different Au/MgO catalysts.

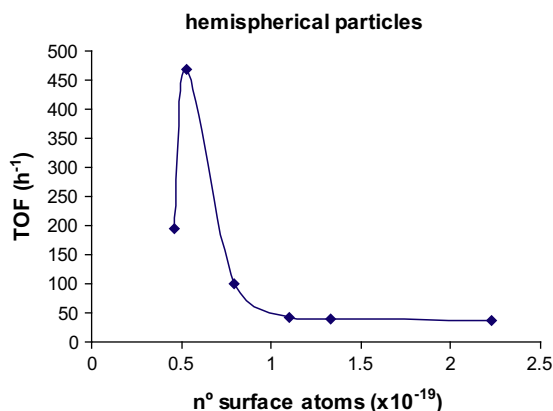


Fig. 8. Turnover frequency (TOF) in h^{-1} for the oxidation of benzyl alcohol at 453 K versus number of surface atoms on the series of Au/MgO catalysts described in Table 3.

tion enthalpies follow the opposite trend. This is in complete agreement with the results obtained from the theoretical study described in Section 3.1 and suggests that the direct relationship between particle size and catalytic activity cannot only be attributed to a larger concentration of undercoordinated Au sites in the smallest particles, but also to the fact that not all undercoordinated Au sites are equally active. To further confirm this hypothesis, turnover frequencies (TOF) were measured at different temperatures for the series of catalysts considered, and the results obtained at 453 K are plotted versus the number of surface metal atoms in Fig. 8. The TOF is defined as the number of molecules reacting per surface active site per unit time and is calculated by dividing the measured initial reaction rate r_0 by the number of surface metal atoms in each particle. It indicates the number of sites, among those accessible, that are active for the reaction under study. The number of surface Au atoms was estimated assuming a hemispherical shape for all particles and a surface density of $13.9 \text{ atoms nm}^{-2}$. The plot of TOF against the number of accessible sites provides information about the reactivity of the accessible sites. If all active sites were equivalent, a horizontal straight line should be obtained. However, Fig. 8 shows that the TOF for benzyl alcohol oxidation is high for particles with a small number of accessible sites, and decreases considerably as the number of accessible sites increases. This behavior of the TOF indicates that the reaction is structure sensitive, that is, that the activity of all the accessible sites is not equivalent, as suggested by the theoretical study presented in the previous section. Therefore, by comparing the experimental kinetic values and the results from calculations, it is found that the design of an active and selective Au catalyst should involve the synthesis of Au particles with size and shape that maximize the number of atoms with the lowest coordination number.

4. Conclusions

The complete molecular mechanism for ethanol oxidation to ethanal has been elucidated from periodic DFT-based calculations carried out on different catalyst models including perfect and stepped single crystal Au surfaces as well as an isolated Au_{38} nanoparticle, which is a prototype for this kind of systems. A clear trend exists in the reactivity of the model surfaces, measured either by the adsorption energy of the adsorbates or by the activation barriers involved in the reaction. These two quantities are indeed linearly correlated in a BEP relationship. Hence, the activation energy decreases (and the adsorption energy increases) with decreasing the Au coordination number. From the model calculations, it can be concluded that not all active sites are equivalent, and that real

gold catalysts might have heterogeneous surfaces, with Au atoms in different coordination state showing different reactivity towards alcohol dehydrogenation. That is, alcohol dehydrogenation on gold catalysts might be a structure-sensitive reaction. This proposal has been experimentally confirmed by measuring the kinetics of benzyl alcohol oxidation on a series of Au/MgO catalysts having different particle diameter and therefore different concentration of low coordinated Au sites. Comparison of the trends observed in DFT calculated alcohol adsorption energies and activation barriers with those found in the values obtained from the kinetic experiments, together with the analysis of the variation of the TOF with the number of accessible Au sites in different samples, allows us to conclude that the oxidative dehydrogenation of alcohols to carbonyl compounds is structure sensitive and that the activity of the accessible Au sites is heterogeneous and varies with the coordination number.

Acknowledgments

We thank Consolider-Ingenio 2010 (project MULTICAT), Spanish MICINN (Projects FIS2008-02238 and MAT2006-14274-C02-01), Generalitat Valenciana (Project PROMETEO/2008/130), Generalitat de Catalunya (grants 2009SGR1041 and XRQTC) and COST Action D41 "Inorganic oxides: surfaces and interfaces" for financial support and Red Española de Supercomputación (RES) for computational resources and technical assistance. J.R. expresses his gratitude to the Mexican CONACyT for a postdoctoral fellowship. T. R. thanks Consejo Superior de Investigaciones Científicas for 13-P fellowships. FI acknowledges support received through the "2009 ICREA Academia" prize for excellence in research.

Appendix A. Supplementary material

Supplementary data associated with this article can be found, in the online version, at [doi:10.1016/j.jcat.2010.11.013](https://doi.org/10.1016/j.jcat.2010.11.013).

References

- [1] R.A. Sheldon, *Catalytic Oxidation*, in: R.A. Sheldon, R.A. van Santen (Eds.), World Scientific Publishing, Singapore, 1995.
- [2] R.A. Sheldon, J.K. Kochi, *Metal-catalyzed Oxidations of Organic Compounds*, Academic Press, New York, 1981.
- [3] T. Mallat, A. Baiker, *Chem. Rev.* 104 (2004) 3027.
- [4] K. Yamaguchi, N. Mizuno, *Angew. Chem. Int. Ed.* 41 (2002) 4538.
- [5] K. Yamaguchi, N. Mizuno, *Chem. Eur. J.* 9 (2003) 4353.
- [6] Z.X. Zhang, P. Chen, J. Liu, Y.H. Zhang, W. Shen, H.L. Xu, Y. Tang, *Chem. Commun.* (2008) 3290.
- [7] K. Shimizu, K. Sugino, K. Sawabe, A. Satsuma, *Chem. Eur. J.* 15 (2009) 2341.
- [8] F. Zacheria, N. Ravasio, R. Psaro, A. Fusi, *Chem. Eur. J.* 12 (2006) 6426.
- [9] L. Huang, Y. Zhu, C. Huo, H. Zheng, G. Feng, C. Zhang, Y. Li, *J. Mol. Catal. A: Chem.* 288 (2008) 109.
- [10] S. Carrettin, P. McMorn, P. Johnston, K. Griffin, G.J. Hutchings, *Chem. Commun.* (2002) 696.
- [11] A. Abad, P. Concepción, A. Corma, H. García, *Angew. Chem. Int. Ed.* 44 (2005) 4066.
- [12] A. Abad, A. Corma, H. García, *Chem. Eur. J.* 14 (2008) 212.
- [13] C. Della Pina, E. Falletta, M. Rossi, *J. Catal.* 260 (2008) 384.
- [14] Y. Guan, E.J.M. Hensen, *Appl. Catal. A: Gen.* 361 (2009) 49.
- [15] K. Mori, T. Hara, T. Mizugaki, K. Ebitani, K. Kaneda, *J. Am. Chem. Soc.* 126 (2004) 10657.
- [16] J.D. Grunwaldt, M. Caravati, A. Baiker, *J. Phys. Chem. B* 110 (2006) 25586.
- [17] D. Ferri, C. Mondelli, F. Krumeich, A. Baiker, *J. Phys. Chem. B* 110 (2006) 22982.
- [18] M. Comotti, C. Della Pina, R. Matarrese, M. Rossi, *Angew. Chem. Int. Ed.* 43 (2004) 5812.
- [19] A. Villa, D. Wang, N. Dimitratos, D.S. Su, V. Trevisan, L. Prati, *Catal. Today* 150 (2010) 8.
- [20] S. Kanaoka, N. Yagi, Y. Fukuyama, S. Aoshima, H. Tsunoyama, T. Tsukuda, H. Sakurai, *J. Am. Chem. Soc.* 129 (2007) 12060.
- [21] T. Ishida, M. Nagaoka, T. Akita, M. Haruta, *Chem. Eur. J.* 14 (2008) 8456.
- [22] H.L. Liu, Y.L. Liu, Y.W. Li, Z.Y. Tang, H.F. Jiang, *J. Phys. Chem. C* 114 (2010) 13362.
- [23] A. Corma, T. Ródenas, M.J. Sabater, *Chem. Eur. J.* 16 (2010) 254.
- [24] A. Quintanilla, V.C.L. Butselaar-Orthlieb, C. Kwakernaak, W.G. Sloof, M.T. Kreutzer, F. Kapteijn, *J. Catal.* 271 (2010) 104.

- [25] J. Radilla, M. Boronat, A. Corma, F. Illas, *Phys. Chem. Chem. Phys.* 12 (2010) 6492.
- [26] J.P. Perdew, J.A. Chevary, S.H. Vosko, K.A. Jackson, M.R. Pederson, D.J. Singh, C. Fiolhais, *Phys. Rev. B* 46 (1992) 6671.
- [27] J.P. Perdew, J.A. Chevary, S.H. Vosko, K.A. Jackson, M.R. Pederson, D.J. Singh, C. Fiolhais, *Phys. Rev. B* 48 (1993) 4978.
- [28] J.P. Perdew, Y. Wang, *Phys. Rev. B* 45 (1992) 13244.
- [29] P.E. Blöchl, *Phys. Rev. B* 50 (1994) 17953.
- [30] G. Kresse, D. Joubert, *Phys. Rev. B* 59 (1999) 1758.
- [31] G. Kresse, J. Furthmüller, *Comput. Mater. Sci.* 6 (1996) 15.
- [32] G. Kresse, J. Furthmüller, *Phys. Rev. B* 54 (1996) 11169.
- [33] H.J. Monkhorst, J.D. Pack, *Phys. Rev. B* 13 (1976) 5188.
- [34] A. Heyden, A.T. Bell, F.J. Keil, *J. Chem. Phys.* 123 (2005) 224101.
- [35] G. Henkelman, H. Jónsson, *J. Chem. Phys.* 111 (1999) 7010.
- [36] E. Sanville, S.D. Kenny, R. Smith, G. Henkelman, *J. Comp. Chem.* 28 (2007) 899.
- [37] G. Henkelman, A. Arnaldsson, H. Jónsson, *Comput. Mater. Sci.* 36 (2006) 254.
- [38] J.N. Brønsted, *Chem. Rev.* 5 (1928) 231.
- [39] M.G. Evans, M. Polanyi, *Trans. Faraday Soc.* 34 (1938) 11.